Performance Enhancement of Plasmonic Sub-Terahertz Detector Based on Antenna Integrated Low-Impedance Silicon MOSFET

Min Woo Ryu, *Student Member, IEEE*, Kwan Sung Kim, Jeong Seop Lee, Kibog Park, Jong-Ryul Yang, *Member, IEEE*, Seong-Tae Han, and Kyung Rok Kim, *Member, IEEE*

***Abstract*— We demonstrate the performance enhancement of field-effect transistor (FET)-based plasmonic terahertz (THz) detector with monolithic integrated antenna in low-impedance regime and report the experimental results of Si MOSFET impedance in THz regime using 0.2-THz measurement system. By designing FET with low-impedance ranges (<1 kΩ) and integrating antennas with impedances of 50 and 100 Ω, we found that our low-impedance MOSFETs have the input impedance criterion of 50 Ω at 0.2 THz and the MOSFETs with thinner gate oxide show the highly enhanced plasmonic photoresponses at 50-Ω antenna by 325 times from the result of the detector without antenna.**

***Index Terms*— MOSFET, plasmonic, terahertz, detector, impedance, photoresponse.**

I. Introduction

TERAHERTZ (THz) wave detectors have been extensively developed to be used in the various applications such as real-time imaging for security and food inspection as well as high data-rate wireless communication [1]. Recently, it is expected that the multi-pixel real-time THz imaging detectors are brought in the near-future by remarkable progress of THz detectors based on CMOS-compatible Schottky barrier diode (SBD) [2] or silicon (Si) field-effect transistor (FET) [3]–[7], since they can be integrated with on-chip antenna and amplifier in a cost-effective way showing a competitive performance to III-V high electron mobility transistor (HEMT) [8], [9].

Plasmonic power detection mechanism based on FET, which is not limited by cut-off frequency as in SBD, has attractive features such as enhanced responsivity {R_v = photoresponse (V)/input THz power (W)} according to the increase of THz frequency [10] and robustness to high input THz power [11]. For sub-micron Si MOSFETs to detect sub-millimeter THz waves, FETs are generally integrated with antennas considering THz wavelength. At this point, careful MOSFET device design considering its input impedance and matching of the antenna is one of the most important issues in high-performance plasmonic THz detectors based on antenna integrated MOSFET. Although a high input impedance of FET is preferable for high responsivity in quasi-static RF analysis [12], it is difficult to realize antenna with ideal power matching because of high impedance [13]. Moreover, the width of the feeding line should become smaller for higher impedance, which results in performance variation by narrow margin of process tolerance. Thus, low-impedance FET can be a promising candidate for wideband multi-pixel detector with uniformly enhanced responsivity by characterizing its impedance exactly pursuing real-time large-area THz imaging. In spite of its significance, the systematic experimental investigations of Si MOSFET impedance in THz regime have not been reported yet.

In this letter, we demonstrate the performance enhancement of plasmonic THz detector based on low-impedance MOSFET with monolithic integrated antenna and report the experimental evidences of FET impedance in THz regime through 0.2-THz measurement system. Si MOSFETs are fabricated with a relatively large size for low impedance and thus, the uniform photoresponse results of the respective detector group are presented to guarantee the measured photoresponse changes only owing to the different antenna input impedances.

II. Device Fabrication and THz Detection Results

Figure 1 (a) and (b) show top-view micrograph images of FET detectors integrated with monolithic patch antenna having the antenna characteristic impedance (Z_a) of 50 and 100 Ω, respectively. As shown in Fig. 1, a width of feeding line is determined from the characteristic impedance (Z_0) and all the other dimensions are designed for detecting 0.2 THz signals by using three-dimensional (3D) electromagnetic simulation. For plasmonic THz detection of FET, antenna feeding lines are connected between gate (signal) and source (ground) of MOSFET and thus, FET gate-to-source input impedance (complex Z_{gs}) should be matched with $Z_a = Z_0$ (real) for smaller reflection and higher photoresponse (Δu) of drain (output) dc voltage. In terms of the matching between

Manuscript received December 28, 2014; accepted January 18, 2015. Date of publication January 21, 2015; date of current version February 20, 2015. This work was supported in part by the Research and Development Convergence Program through the Ministry of Science, ICT and Future Planning and Korea Research Council for Industrial Science and Technology, Korea, under Grant B551179-09-05-00, and in part by the Pioneer Research Center Program through the National Research Foundation of Korea within the Ministry of Science, ICT and Future Planning under Grant 2012-0009594. The review of this letter was arranged by Editor M. Rais-Zadeh.

M. W. Ryu, K. S. Kim, J. S. Lee, K. Park, and K. R. Kim are with the School of Electrical and Computer Engineering, Ulsan National Institute of Science and Technology, Ulsan 689-798, Korea (e-mail: krkim@unist.ac.kr).

J.-R. Yang and S.-T Han are with Korea Electrotechnology Research Institute, Ansan 426-170, Korea.

Color versions of one or more of the figures in this letter are available online at http://ieeexplore.ieee.org.

Digital Object Identifier 10.1109/LED.2015.2394446

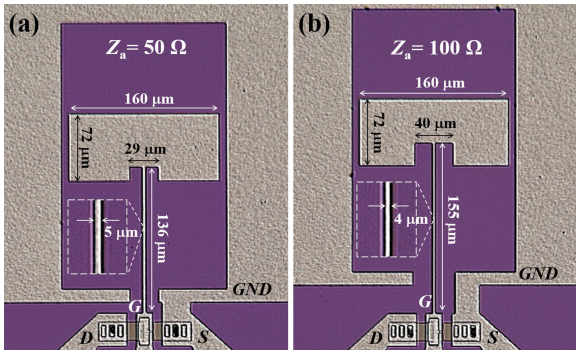

Fig. 1. Top-view micrograph images of the fabricated plasmonic THz detector based on Si MOSFET with monolithic integrated patch antennas: (a) antenna characteristic impedance of $Z_a = 50\ \Omega$ and (b) $Z_a = 100\ \Omega$.

complex Z_{gs} and real $Z_a = Z_0$ with the feeding (transmission) lines, the equivalent transmission line model with the multiple reflection coefficient (Γ_m) should be considered and the matching condition given by

$$|Z_{gs}| = Z_0 \quad for \quad \Gamma_m = 0 \tag{1}$$

only with $|Z_{gs}|$ (magnitude of complex Z_{gs}) can be derived from the equivalent quarter-wave transformer circuit analysis [14]. Therefore, higher Δu by smaller Γ_m means that $|Z_{gs}|$ become more close to $Z_a = Z_0$ from Eq. (1). For low-Z_{gs} Si MOSFET, the large micron-dimensions are simply applied to the asymmetric source ($W_S = 2\ \mu$m) and drain width ($W_D = 10W_S$) based on non-self-aligned gate-last process with gate length of $L = 2\ \mu$m. The details of the asymmetric Si MOSFET fabrication can be found in our previous work [7].

Figure 2 (a) shows our experimental setup of THz detection for Δu measurement of the fabricated detector. Diverging Gaussian beam with 0.2-THz radiation was generated by a gyrotron source in higher-order mode resonator, which enables a large-area real-time detection with the continuous-wave (CW) method since it is stable in sub-THz frequency regime [15]. After the focused THz beam is passing through chopper hole by off-axis parabola (OAP) mirrors, diverging THz beam with a full-width at half-maximum (FWHM) of 40 mm (inset) with attenuated source power ($P_s \sim 1$ W) is absorbed by antenna, which transferred it to FET gate as an ac signal. Finally, dc Δu is measured by SMU (Agilent B2912A) through the background noise reduction using lock-in amplifier (SR830) by bandpass filtering around the chopper modulation frequency. Considering actual detector area ($A_d = 173 \times 280\ \mu m^2$, cf. beam area $A_{beam} = \pi(20)^2$ mm^2), the actual power ($P_a = P_s \times A_d / A_{beam}$) on the antenna-integrated detector can be estimated as 0.038 mW.

The measured Δu results of our low-Z_{gs} MOSFET are plotted in Fig. 2 (b). According to a non-resonant plasmonic detection theory [10], the peak points of Δu are observed in subthreshold region before the zero gate overdrive voltage (V_{GS}-$V_T = 0$ V). Interestingly, based on the same MOSFETs with uniform dc I-V curves from 10 samples, the distinguished group of the peak Δu values (i.e. detecting performance) are clearly observed by two different Z_a values. It should be noted that Δu enhancement according to the

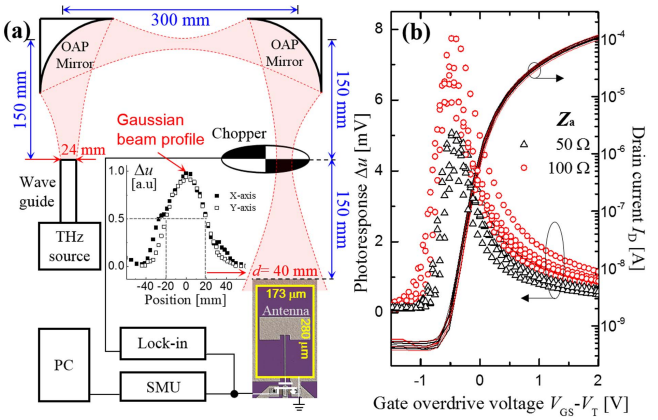

Fig. 2. (a) Experimental setup for plasmonic THz detector using 0.2-THz gyrotron with Gaussian beam profile (inset). (b) Experimental results of uniform dc I_D-V_G curves from the same MOSFETs (10 samples) at $V_D = 50$ mV and the photoresponse as a function of the gate overdrive voltage $V_{GS} - V_T$ for different antennas with $Z_a = 50\ \Omega$ and 100 Ω (5 samples for each group).

TABLE I
DEVICE PARAMETERS OF LOW-Z_{gs} Si MOSFET SAMPLES WITH $L = W_S = W_D/10$

MOSFET	T_{ox} (nm)	Junction depth (nm)	Expected Z_{gs} (Ω)
Sample *A*	50	250	< 1 k (low)
Sample *B*	50	750	< 100 (lower)
Sample *C*	10	300	< 100 (lower)

increase of Z_a from 50 Ω to 100 Ω provide an experimental evidence of the fabricated Si MOSFET input impedance of $Z_{gs} > 50\ \Omega$ close to 100 Ω in 0.2-THz frequency.

III. PERFORMANCE ENHANCEMENT AND DISCUSSION

For more systematic experiments on MOSFET impedance, different samples of low-Z_{gs} Si MOSFET are also taken as summarized in Table I. Based on the same layout dimensions with the reference sample *A*, which is presented in Fig. 2(b), lower-Z_{gs} MOSFETs can be expected by increasing capacitance with junction broadening from 250 nm to 750 nm junction depth in sample *B* and thinner gate oxide thickness (T_{ox}) in sample *C*. These expected trends toward lower Z_{gs} in our Si MOSFET samples are confirmed by TCAD device simulation using two-port network analysis as shown in Fig. 3. The estimated Z_{gs} (magnitude of complex impedance) of our low-impedance MOSFETs is below 1 kΩ around 0.2 THz, while the conventional nanoscale MOSFETs with smaller device dimensions ($L = W = 45$, 65, 130 nm, $T_{ox} = 2.2 \sim 3.2$ nm [16]) show high Z_{gs} above 1 kΩ, which is reasonable range when compared with low-Z_{gs} level in the multi-fingered (finger number $NF > 10$) RF MOSFETs [17] and single-fingered 130-nm MOSFETs with larger widths [18].

These estimated impedance ranges of our MOSFET samples ($Z_{gs} < 1$ kΩ) have been experimentally demonstrated in Fig. 4, which present the extracted peak Δu results from the respective detector sample group (15 samples) combined with each Z_a split of 50 and 100 Ω. As observed in Fig. 2(b), MOSFET sample *A* with the estimated $Z_{gs} < 1$ kΩ shows the higher Δu at $Z_a = 100\ \Omega$ than those at $Z_a = 50\ \Omega$ here confirmed by multiple uniform samples while sample *B* group with lower-expected $Z_{gs} < 100\ \Omega$ shows the lower Δu at

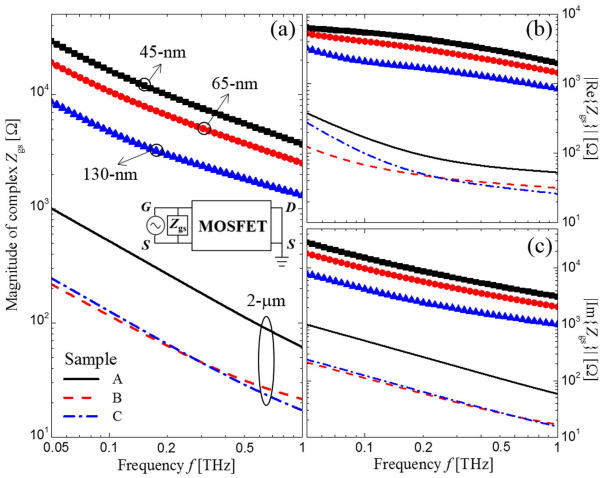

Fig. 3. TCAD simulation results of Z_{gs} by two-port network analysis in the frequency range from 50 GHz to 1 THz for our low-impedance FETs and conventional nanoscale FETs. For each simulation, gate overdrive voltage of V_{GS}-V_T is −0.1 V. (a) Magnitude, (b) Real and (c) Imaginary part of Z_{gs}.

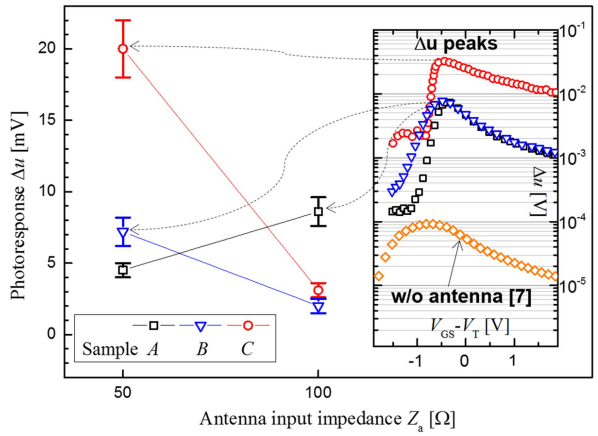

Fig. 4. Extracted Δu peaks from each detector sample group combined with Z_a splits of 50 Ω and 100 Ω. Inset shows Δu as a function of V_{GS}-V_T for each sample with maximum Δu peaks compared with detector without antenna [7]. Symbols and error bars show the average and standard deviation from 15 samples of each detector group, respectively.

$Z_a = 100$ Ω than sample A and more enhanced Δu at $Z_a = 50$ Ω. Since there is no difference of T_{ox} and the plasmonic channel electron density modulation between sample A and B, it can be concluded that this result is the experimental evidence of the FET input impedance range in that Z_{gs} of sample $B < 50$ Ω while Z_{gs} of sample $A > 50$ Ω.

Sample C group shows more highly enhanced Δu with best $R_v = 32$ mV/0.038 mW = 842 V/W at $Z_a = 50$ Ω (325 times) than those of sample B (75 times) from the result of the detector without antenna as shown in inset from Ref. [7], even if sample B and C have same criterion of $Z_{gs} < 50$ Ω as expected in Fig. 3. The lowest noise-equivalent-power (NEP) in sample C (inset) has been obtained as 18 pW/$\sqrt{\text{Hz}}$ at V_{GS}-$V_T = 0.25$ V commonly based on the channel thermal noise ($N = (4kTR_{ch})^{0.5}$), which is comparable with the reported lowest NEP values for antenna-coupled plasmonic Si-based THz detectors [3], [19], owing to the relatively low channel resistance (R_{ch}) from large micron-scale width for low-impedance MOSFET design. It can be noted that these enhancement trends of R_v and NEP in sample C with thinner T_{ox} mainly originate from increase of the plasmonic channel electron density modulation by T_{ox} scaling. Therefore, MOSFET for plasmonic THz detectors should be designed by considering both external impedance and internal plasmonics of the non-quasi-static channel electron density modulation.

IV. Conclusion

Performance enhancement of Si MOSFET-based plasmonic THz detector has been demonstrated with monolithic integrated antenna and the impedance range of Si MOSFET presented in THz regime using 0.2-THz measurement system. Significant effects of FET and antenna input impedances on the detecting performance provide the guideline to design FET plasmonic THz detectors in low impedance range based on the enhancement of plasmonic channel electron density.

References

[1] P. H. Siegel, "Terahertz technology," *IEEE Trans. Microw. Theory Techn.*, vol. 50, no. 3, pp. 910–928, Mar. 2002.
[2] R. Han *et al.*, "Active terahertz imaging using Schottky diodes in CMOS: Array and 860-GHz pixel," *IEEE J. Solid-State Circuits*, vol. 48, no. 10, pp. 2296–2308, Oct. 2013.
[3] F. Schuster *et al.*, "Broadband terahertz imaging with highly sensitive silicon CMOS detectors," *Opt. Exp.*, vol. 19, no. 8, pp. 7827–7832, Apr. 2011.
[4] H. Sherry *et al.*, "A 1 k pixel CMOS camera chip for 25 fps real-time terahertz imaging applications," in *ISSCC Tech. Dig. Papers*, 2012, pp. 252–254.
[5] A. Lisauskas *et al.*, "Terahertz responsivity and low-frequency noise in biased silicon field-effect transistors," *Appl. Phys. Lett.*, vol. 102, no. 15, pp. 153505-1–153505-4, Apr. 2013.
[6] A. Gutin *et al.*, "Modeling terahertz plasmonic Si FETs with SPICE," *IEEE Trans. THz Sci. Technol.*, vol. 3, no. 4, pp. 545–549, Sep. 2013.
[7] M. W. Ryu *et al.*, "Photoresponse enhancement of plasmonic terahertz wave detector based on asymmetric silicon MOSFETs with antenna integration," *Jpn. J. Appl. Phys.*, vol. 53, no. 4S, pp. 04EJ05-1–04EJ05-4, Apr. 2014.
[8] J.-Q. Lu *et al.*, "Terahertz detector utilizing two-dimensional electronic fluid," *IEEE Electron Device Lett.*, vol. 19, no. 10, pp. 373–375, Oct. 1998.
[9] M. Bialek *et al.*, "Plasmonic terahertz detectors based on a high-electron mobility GaAs/AlGaAs heterostructure," *J. Appl. Phys.*, vol. 115, no. 21, pp. 214503-1–214503-8, Jun. 2014.
[10] M. Dyakonov and M. Shur, "Detection, mixing, and frequency multiplication of terahertz radiation by two-dimensional electronic fluid," *IEEE Trans. Electron Devices*, vol. 43, no. 3, pp. 380–387, Mar. 1996.
[11] V. Y. Kachorovskii *et al.*, "Performance limits for field effect transistors as terahertz detectors," *Appl. Phys. Lett.*, vol. 102, no. 22, pp. 223505-1–223505-5, Jun. 2013.
[12] E. Ojefors *et al.*, "A 0.65 THz focal-plane array in a quarter-micron CMOS process technology," *IEEE J. Solid-State Circuits*, vol. 44, no. 7, pp. 1968–1976, Jul. 2009.
[13] U. R. Pfeiffer *et al.*, "Toward low-NEP room-temperature THz MOSFET direct detectors in CMOS technology," in *Proc. 38th IRMMW-THz*, Sep. 2013, pp. 1–2.
[14] D. M. Pozar, *Microwave Engineering*. Hoboken, NJ, USA: Wiley, 2005, pp. 73–79.
[15] A. C. Torrezan *et al.*, "Continuous-wave operation of a frequency-tunable 460-GHz second-harmonic gyrotron for enhanced nuclear magnetic resonance," *IEEE Trans. Plasma Sci.*, vol. 38, no. 6, pp. 1150–1159, Jun. 2010.
[16] (2001). *International Technology Roadmap for Semiconductors*. [Online]. Available: http://public.itrs.net
[17] S. P. R. Bandi *et al.*, "Effect of gate poly-silicon depletion on MOSFET input impedance," *IEEE Microw. Wireless Compon. Lett.*, vol. 16, no. 5, pp. 290–292, May 2006.
[18] S. Domingues *et al.*, "Analysis of CMOS 0.13 μm test structures for 0.6 to 1.5 THz imaging," in *Proc. IRMMW-THz*, Sep. 2013, pp. 1–2.
[19] M. Bauer *et al.*, "Antenna-coupled field-effect transistors for multi-spectral terahertz imaging up to 4.25 THz," *Opt. Exp.*, vol. 22, no. 16, pp. 19235–19241, Aug. 2014.